Hindawi
Shock and Vibration
Volume 2018, Article ID 4073963, 15 pages
https://doi.org/10.1155/2018/4073963

Research Article

Use of a Simple Mechanical Analogy to Analytically Tune the PD Controller of a Flexible Manipulator System

Sang-Myeong Kim,[1,2] **Heungseob Kim**,[1] **and Kwangsuck Boo**[1]

[1]*High Safety Vehicle Core Technology Research Center, Inje University, 607 Obang-dong, Gimhae 621-749, Republic of Korea*
[2]*Mechanical Engineering Department, UNESP, Ilha Solteira 15385-000, Brazil*

Correspondence should be addressed to Sang-Myeong Kim; ksmnaver@naver.com

Received 30 June 2018; Accepted 18 September 2018; Published 18 November 2018

Academic Editor: Franck Poisson

A study is presented in this paper that uses a simple mechanical analogy to analytically tune the PD (proportional-derivative) controller of a linear flexible manipulator system. More specifically, the aim is to give simple closed-form solutions of the optimal P and D gains to yield the maximum bandwidth under a given damping requirement *or* conversely the maximum damping under a given bandwidth requirement. The idea of this study is based on the observation that the performance of the complete manipulator system is largely determined by the operational dynamics of the fundamental vibration mode. A lumped element method is thus applied to model this dynamics in terms of simple lumped mechanical elements. It subsequently turns out that the original servo control problem is analogous to a conventional Zener mount design problem, that is, mathematically, to optimize a third-order dynamic system consisting of the Zener model of a viscoelastic mount and an inertial object upon it. A design methodology is finally established to analytically determine the optimal elements of the mount, corresponding to the optimal control gains. Simulations and experiments were also conducted with a single-link flexible beam to support the model and the design methodology developed.

1. Introduction

There are various methods to tackle vibration problems of a flexible manipulator system [1], which is a servo machine having a flexible joint or link. They include tuning methods of PD (proportional-derivative) gains [2] and PID (proportional-integral-derivative) gains [3]; feedforward control methods using various filters including input shaping [4], notch [5], and inverse [6] filters; and feedback control methods using additional vibration sensors such as an accelerometer [7]. Amongst, the PD-tuning method is the simplest and is of interest throughout this paper. It is particularly suitable for linear [8] and linearized [9, 10] manipulator systems, where no nonlinear dynamic effects (e.g., gravity and friction effects) are present. An understanding of this is important for control engineers as it is also a prerequisite to an understanding of the PID-tuning method that is then for general nonlinear manipulator systems.

Irrespective of the methods listed above, the fundamental vibration mode of the complete servo machine plays a key role in determining the system performance [1, 6]. The PD-tuning method is basically to tune the vibration frequency and the damping property of this mode, which are closely related to the bandwidth (i.e., speed) and damping (i.e., settling time) requirements of the system, respectively. The PD-tuning method is thus to give an optimal servo machine in terms of both speed and settling time. If an excessive speed had to be practiced due to some other requirements, this mode could then be suppressed by an additional means such as a control method. The control methods listed earlier are thus generally for rapid servo machines, which are nonoptimal in the sense of gain-tuning. The study presented in this paper is specifically concerned with the PD-tuning method for linear servo machines that are further nonrapid. Unlike the situation for rigid manipulators [2, 11], analytical studies towards the optimal PD gains for flexible manipulators are scarce in the literature. Instead, numerical and empirical tuning methods have been exclusively practiced by inspecting, for

example, step responses. However, these are trial-and-error practices whose repetitions would not necessarily help engineers to build up an understanding of the dynamics and control mechanisms involved.

An analytical study is thus conducted in this paper that uses a simple mechanical analogy to determine the optimal gains. More specifically, the aim of this study is to give simple closed-form solutions of the optimal P and D gains to yield the maximum bandwidth under a given damping requirement *or* conversely the maximum damping under a given bandwidth requirement. To model the operational dynamics of the fundamental vibration mode, the lumped element method (LEM) [12–14] is applied to transform the mechanical manipulator into a system consisting of a base mass, an appendage mass, and a resilient member connecting the two masses [15]. The P and D gains are then, respectively, transformed to a spring and a damper underneath the base mass, thus yielding a simple positive-definite two-body lumped element system (LES) representing the complete flexible manipulator system. Because the dynamic effect of the base mass can be ignored by implementing a large P gain, which is an interesting finding, the original servo control problem is eventually transformed into a conventional viscoelastic mount design problem dealing with a one-body LES. More precisely it is, in fact, a Zener mount design problem [16, 17], where a given inertial object (the manipulator inertia) is supported by a Zener mount that is comprised of a given spring (the manipulator flexibility) in series with a parallel connection of another spring (P gain) and a damper (D gain). A design methodology is finally established by adapting the conventional design rule of the Zener mount system [18, 19], to analytically determine the optimal P and D gains.

The paper is organized as follows. Section 2 describes the modeling process to simplify the servo control problem to a Zener mount design problem. Section 3 describes the design (tuning) process to determine the optimal elements of the Zener mount, corresponding to the optimal P and D gains. New indexes are also proposed to quantitatively specify the system bandwidth and damping requirements. Simulation and experimental work are described in Section 4, followed by some conclusions in Section 5. There are also two appendices in this paper to summarize some important frequencies used in the modeling and design processes and also to review and compare two other alternative Zener mount design methods based, respectively, on convex minimization and frequency tuning.

2. Modeling

2.1. Lumped Element Modeling. Consider a servo positioning system driving a flexible manipulator in the horizontal plane as shown in Figure 1(a), where the beam represents the flexible manipulator. The motor rotor x_1 is PD-controlled using the P gain k and the D gain c to locate the tip x_2 at the position set by the command input x_0. The P and D gains are generally related to the speed and the settling time of the servo machine, respectively. The Laplace operator is denoted by s. A command force input f is additionally shown for completeness. It is assumed throughout this paper that the dynamics of the mechanical manipulator are linear (*Condition* I: linearity).

Applying the novel LEM [12–14], the low-frequency operational dynamics of the mechanical manipulator can be closely approximated, as shown in Figure 1(b), by using a semidefinite system consisting of the base mass m, the appendage mass m_a, and a resilient member (a parallel connection of a spring k_a and a damper c_a) connecting the two masses. A series connection may alternatively be used. The oscillator (m_a, c_a, and k_a) represents the first vibration mode of the beam in the fixed-free boundary condition. The physical variables are used in a generalized sense so that the force (f) can mean a force or a torque; and the motions (x_1 and x_2) can be translational or rotational. The frequency dependence $e^{j\omega t}$ of these variables has been suppressed for simplicity, where $j = \sqrt{-1}$, ω is the angular frequency, and t is the time. Similarly, physical quantities are used in a generalized sense so that a mass can mean a moment of inertia; and the translational springs and dampers indicated can mean rotational springs and dampers, respectively.

Since the PD controller considered is a passivity-based controller [13], the control gains k and c can be, respectively, transformed into a spring and a damper underneath the base mass m so as to complete the model of the positive-definite two-body LES representing the complete manipulator system including the servo actuation part. A hypothesis implicitly used here is that the servo actuator is nonrapid (not a very large k) such that it cannot excite any higher order modes of the mechanical manipulator but only the first one (*Condition* II: nonrapid operation).

Applying now the impedance approach [20–22], it is convenient to regard the two-body LES as a coupled system between the base and the appendage as indicated in Figure 1(b). The base impedance is given by

$$Z_B = j\omega m + c + \frac{k}{j\omega}, \tag{1}$$

where $k = c = 0$ if uncontrolled. Thus, Z_B is variant depending on the control gains used. In contrast, the appendage impedance is fixed and can be written as

$$Z_A = j\omega m_a T_{12}, \tag{2}$$

where the vibration transmissibility $T_{12} = x_2/x_1$ is given by

$$T_{12} = \frac{\omega_a^2 + j2\zeta_a\omega_a\omega}{\omega_a^2 - \omega^2 + j2\zeta_a\omega_a\omega}, \tag{3}$$

where $\omega_a = \sqrt{k_a/m_a}$ is the angular natural frequency and $\zeta_a = c_a/(2\sqrt{m_a k_a})$ is the damping ratio of the uncoupled appendage. Similarly, those of the uncoupled base can be written as $\omega_b = \sqrt{k/m}$ and $\zeta_b = c/(2\sqrt{mk})$, respectively. The transmissibility defined above is a useful term, which is also widely used in the field of vibration isolation, to assess the vibration transmission characteristic between two points of a vibration system [23]. The impedance of the combined system seen by the source f can then be written as

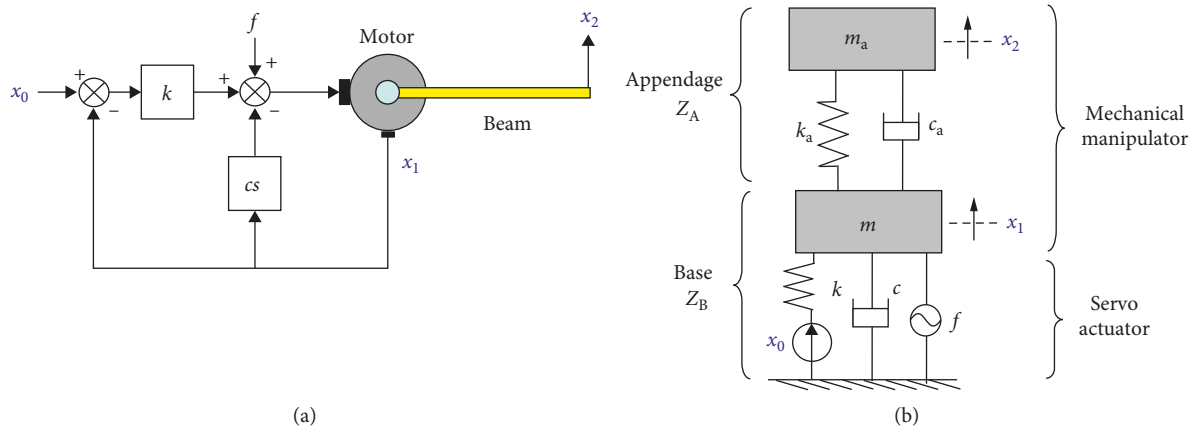

FIGURE 1: PD control of a flexible manipulator with the proportional gain k and the derivative gain c (a) and the equivalent two-body LES (b): x_0 is the command input position, x_1 is the hub position, and x_2 is the tip position.

$$Z = Z_B + Z_A. \tag{4}$$

The combined system without control can be identified by curve-fitting this impedance expression to the measured impedance response [12, 13], as experimentally demonstrated in Section 4. The combined system with control can then be easily predicted by specifying the gains k and c used. As such, a complex-shaped manipulator system even with multiple links can be similarly identified. In fact, the LEM, more fundamentally the impedance approach, is a general approach that can be applied to any linear, passive operational dynamic systems that the conventional Newtonian method (i.e., the mobility approach) is also applicable [14].

If the system is now operated by the motion source x_0 only, the vibration transmissibility from x_0 to x_1 (i.e., the hub position) can be written as

$$T_{01} = \frac{k/j\omega}{Z_A + Z_B}, \tag{5}$$

and that to x_2 (i.e., the tip position) is given by

$$T_{02} = T_{01} \cdot T_{12}, \tag{6}$$

where $T_{01} = x_1/x_0$, $T_{02} = x_2/x_0$, and $T_{12} = x_2/x_1$. Overall, the modeling process can be summarized as follows: given the (measured or simulated) driving point frequency response data of Z at the hub of a manipulator, the LEM is applied to identify the elements (m_a, c_a, k_a, and m) of the LES; and then the complete LES further incorporating the control gains (k and c) is used to predict the hub and tip responses.

2.2. Coupling Analysis. The dynamic behavior of the two-body LES is greatly dependent on the strength of coupling between the two subsystems. As an extreme case, the criterion for weak coupling can be written as $|Z_B| \gg |Z_A|$ [21]. For the specific base system of the variant spring k with the fixed mass m, this criterion can be more conveniently rewritten as

$$\omega_b \ll \omega_a, \tag{7a}$$

$$\omega_a \ll \omega_b. \tag{7b}$$

The former is the case when the servo actuator has a very small operation bandwidth (a very small k) far below the appendage natural frequency ω_a. The latter is the case when it has a very large operation bandwidth (a very large k) far above ω_a. In both cases, the base damper c is little helpful for dissipating the appendage vibration. If the coupling is now made to be strong by appropriately adjusting k (consequently ω_b), which means that Equation (7) no longer holds, it is then possible to dissipate the appendage vibration by using c. This is because the mode being formed is now a global mode. This is the characteristic that is exploited throughout this paper. It is also fortunate that the range of k suggested here (i.e., neither very small nor very large) does not disobey Condition II.

To support the discussion above, Figures 2(a), 2(c), and 2(e) and Figures 2(b), 2(d), and 2(f) show the magnitudes of the transmissibility functions T_{01} and T_{02} for the system in Figure 1(b), respectively. Three values of the base damping ratio ζ_b were tested for three values of the coupling term ω_b/ω_a. The *resonance frequency* ω_r (i.e., the first peak frequency) and the damping property of the fundamental vibration mode of T_{02} are closely related to the bandwidth and the damping requirement of the complete operational manipulator system, respectively. It can be seen in Figures 2(a) and 2(b) that if the strength of coupling is weak (e.g., $\omega_b/\omega_a = 10$), the base damper has very little effect on the fundamental mode. It can also be seen in Figures 2(c) and 2(d) that, for a stronger coupling (e.g., $\omega_b/\omega_a = 3$), the system damping improves but the bandwidth diminishes. The maximum coupling case ($\omega_b/\omega_a = 1$) shown in Figures 2(e) and 2(f) is a special case, where the base system acts as "a *suspending* dynamic vibration absorber" to maximally damp the tip vibration of the appendage [24]. It can though be seen that the bandwidth greatly diminishes. Thus, there is a trade-off between the system damping and the system bandwidth; the damping can only be increased by compromising the bandwidth, and vice versa. These observations are theoretically verified later in this paper.

2.3. Model Reduction by Eigenvalue Analysis. From the discussion in the previous subsection, it is clear that the

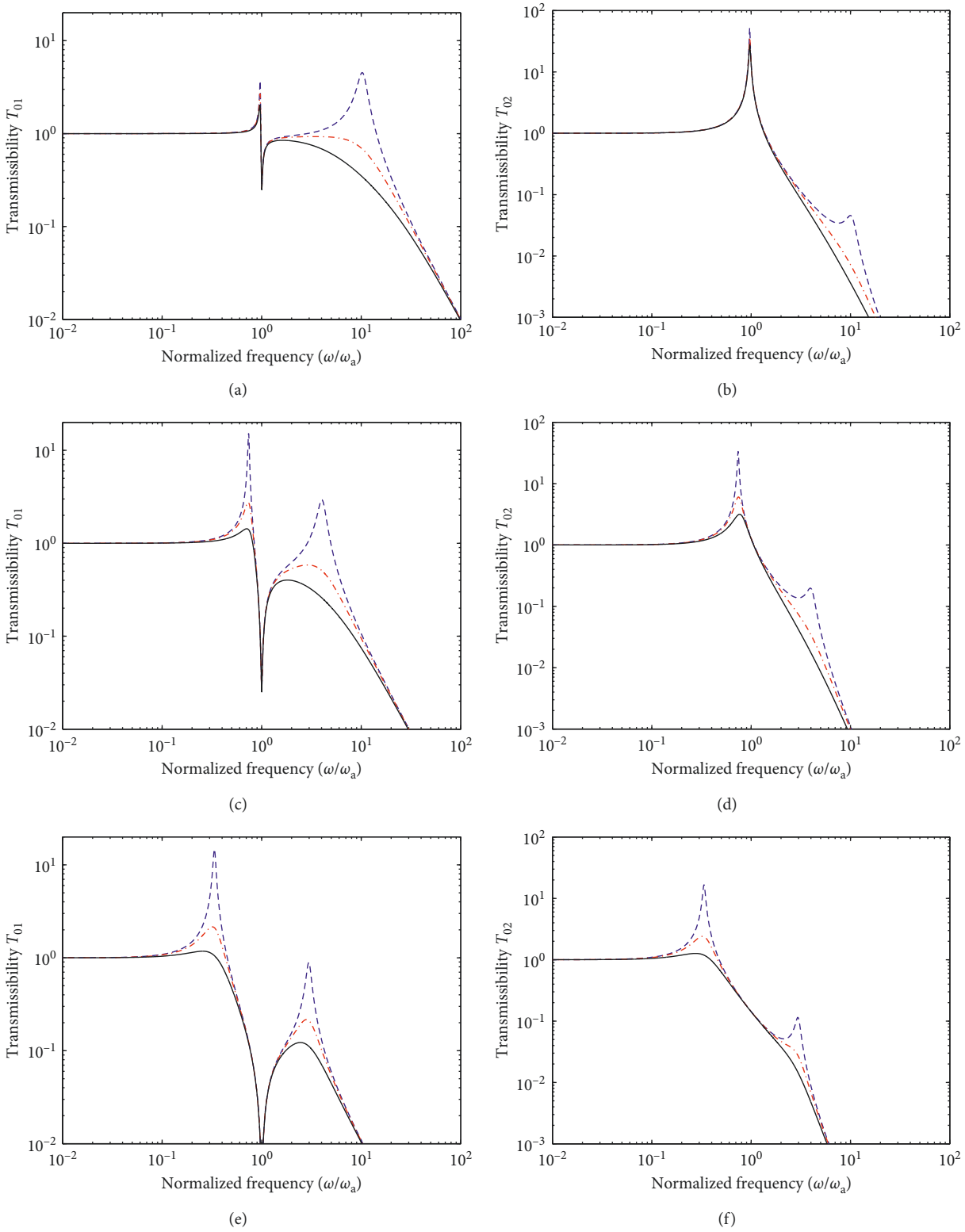

FIGURE 2: Transmissibility functions in magnitude $T_{01} = x_1/x_0$ (a, c, e) and $T_{02} = x_2/x_0$ (b, d, f) for the two-body LES in Figure 1(b) with $\sigma = m_a/m = 7$ and $\zeta_a = 0.01$. Three base damping ratios $\zeta_b = 0.1$ (dashed lines), $1/\sqrt{2}$ (dashed dot), and $\sqrt{2}$ (solid) were tested for each of the three coupling cases $\omega_b/\omega_a = 10$ (a, b), 3 (c, d), and 1 (e, f).

proximity between the two natural frequencies, ω_a and ω_b, can mean the strength of coupling. There are two values of k to give the same proximity: a large k is desirable such that $\omega_a < \omega_b$ (Figure 2); a small k would result in a small bandwidth as it yields $\omega_r < \omega_b < \omega_a$ (not shown in Figure 2). This suggests an important design guideline as follows (*Condition* III: nonslow operation):

$$\omega_a < \omega_b. \tag{8}$$

Equivalently, it can be rewritten as $\kappa < \sigma$ or $m\omega_a^2 = k_{min} < k$ in which $\kappa = k_a/k$ and $\sigma = m_a/m$. Note that this guideline sets the lower bound k_{min} of the P gain. Its upper bound is then limited by Condition II as well as the strength of coupling.

Under the condition given by Equation (8), it is *remarkable* that the two-body LES in Figure 1(b) can be further reduced to the one-body LES shown in Figure 3(a) for the fundamental vibration mode and then to that in Figure 3(b) for the second vibration mode. The appendage damping has been ignored for simplicity. To justify these model reductions, Figure 4 compares the natural frequencies of the two one-body LESs with the exact ones obtained by solving the eigenvalue problem of the original two-body LES for a spring ratio of $\kappa_o = 1$ (a constant), according to the mass ratio σ (a variable). The region $\kappa_o < \sigma$ is shaded. It can be seen that the exact (solid lines) and approximate (dashed) eigenvalues agree well within the shaded region; the agreement gets better as σ increases (i.e., as k increases). Thus, it can be stated that the two one-body LESs shown in Figures 3(a) and 3(b) are reasonable models if Equation (8) holds. A similar discussion can be made when the mass ratio is fixed: σ_o (a constant). The natural frequency of the first LES in Figure 3(a) is henceforth called the *nominal natural frequency* of the fundamental vibration mode and is denoted by $\omega_n = \sqrt{k_{eq}/m_a}$, where $k_{eq} = kk_a/(k + k_a)$ is the static stiffness.

Overall, it has been shown that the design guideline given by Condition III has naturally acted as the model reduction condition to the one-body LES. The first one-body LES shown in Figure 3(a) is a simple mechanical analogy to the operational dynamics of the fundamental vibration mode of a complete flexible manipulator system. Here, the first LES model together with Conditions I–III is an important contribution of this paper. A merit of this is that it is now simple enough to offer a rigorous definition and a subsequent solution of the relevant optimal design problem of the system, as presented in the following section.

3. Optimal Design

3.1. Background. Of interest in this section is the simple one-body LES shown in Figure 3(a), where m_a and k_a mean the inertia and the flexibility of a given mechanical manipulator, respectively. It is *striking* to note that the mount $(k_a - (k\|c))$ is, in fact, the series-type Zener model often used for describing the dynamic behavior of a viscoelastic material [16], where $-$ and $\|$, respectively, indicate a series and a parallel connection of impedances. Such a mount that can be modeled by the Zener model may be called a *Zener mount*, whereas the complete vibration system further containing

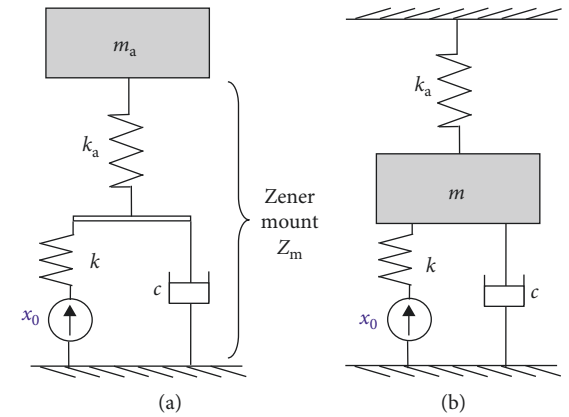

Figure 3: One-body LESs representing the first (a) and the second (b) mode of the two-body LES in Figure 1(b). The system in (a) is specifically called a Zener mount system.

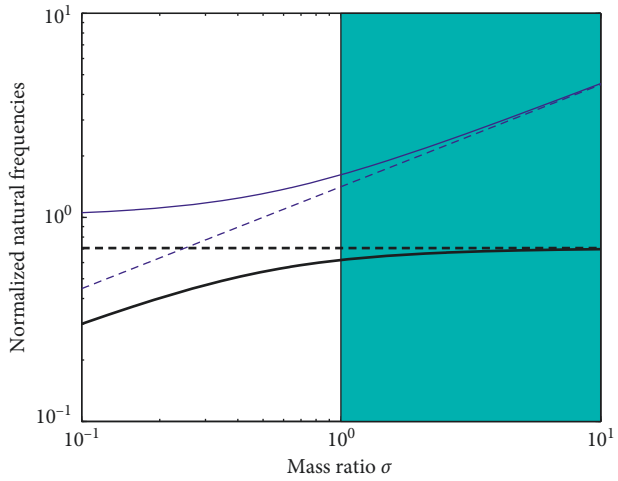

Figure 4: Exact (solid lines) and approximate (dashed) natural frequencies of the first (thick lines) and the second (thin) modes normalized by ω_a for the two-body LES with the fixed spring ratio of $\kappa_o = 1$. The region, where $\kappa_o < \sigma$, is shaded.

the inertial object m_a is called in this paper a *Zener mount system*. The control problem here is also to somehow optimally tune the two elements (k and c) in consideration of the residual transient vibration of m_a. Thus, it can be seen that the original servo control problem is analogous to a conventional Zener mount design problem. An advantage of this analogy is that the linear vibration theory established in the field of vibration isolation can also be applied to study the dynamics of the servo control system in the field of motion control. More specifically, the conventional design rule of a Zener mount system [18, 19] can now be applied to design the optimal PD controller. This task is undertaken in this section for the particular form of the Zener mount system shown in Figure 3(a), where m_a and k_a are fixed and known while k and c are tunable and unknown. As can be seen in what follows, it is a nontrivial but challenging task because the rule appears yet rather a loosely-defined concept on how to solve than any closed-form solution ready to use.

Prior to optimal design, we thus first review the dynamic behavior of the Zener mount in Figure 3(a) whose impedance can be conveniently written as

$$Z_{\mathrm{m}} = \left(\frac{k_{\mathrm{a}}}{j\omega}\right) \cdot C(\omega), \tag{9}$$

where $C(\omega) = \alpha(1 + j\omega X)/(1 + j\alpha\omega X)$, $\alpha = (1 + \kappa)^{-1}$, $X = c/k$, and again $\kappa = k_{\mathrm{a}}/k$. A parallel-type Zener model can also be similarly represented. The complex modulus of the material (i.e., mount) is $k_{\mathrm{a}} \cdot C(\omega)$, whose real and imaginary parts indicate the dynamic (frequency-variant) stiffness and loss functions, respectively. The stiffness function is related to the static and dynamic load-carrying capabilities while the loss function is to the damping capability. It is interesting that the material behavior is completely determined by the lead compensator $C(\omega)$ whose characteristics are well known in the control society [2].

As an illustration, Figure 5 displays the polar, phase, and amplitude responses of a lead compensator for $\alpha = (1 + \kappa_o)^{-1}$ with $\kappa_o = 1$. The loss angle and factor functions of the material can be, respectively, defined by $\delta(\omega) = \angle C(\omega)$ and $\eta(\omega) = \tan(\delta(\omega))$, where the latter is also $\eta(\omega) = \mathrm{Im}[C(\omega)]/\mathrm{Re}[C(\omega)]$. Since the loss factor is more fundamental and general than the damping ratio, it has been widely used in evaluating a viscoelastic material [25]. The transition frequency $\omega_{\mathrm{t}} = (\sqrt{\alpha}\, X)^{-1}$ is critically important in mount design since it is the frequency offering the maximum use of the dynamic loss capability with respect to the dynamic stiffness capability. The maximum loss angle and factor at this frequency are then, respectively, given by $\delta_{\max} = \sin^{-1}([1 - \alpha]/[1 + \alpha])$ and $\eta_{\max} = (1 - \alpha)/(2\sqrt{\alpha})$ [2]. It is noteworthy that either one of α and $\eta_{\max}$ is uniquely determined by the other, which fact will later be used to give a practical definition of the optimization problem. There is also a frequency giving the maximum loss itself, denoted by ω_{l} in Figure 5(a). A mount is seldom tuned to this frequency as it induces a large increase in the dynamic stiffness but a small increase in the dynamic loss, compared with those at ω_{t}.

3.2. Problem Definition and Solution. We then consider the optimal design of the Zener mount system that is a combined system between the inertial object m_{a} and the Zener mount Z_{m}, as shown in Figure 3(a). From the dynamic equation $(j\omega m_{\mathrm{a}} + Z_{\mathrm{m}})v_2 = 0$ with v_2 being the velocity of the inertial object, the characteristic equation can be written in the frequency domain as

$$-\omega^2 m_{\mathrm{a}} + k_{\mathrm{a}}(\mathrm{Re}[C(\omega)])(1 + j\eta(\omega)) = 0, \tag{10a}$$

and more explicitly in terms of $s = j\omega$ as

$$s^3 + (\alpha X)^{-1} s^2 + \omega_{\mathrm{a}}^2 s + X^{-1}\omega_{\mathrm{a}}^2 = 0. \tag{10b}$$

In general, this cubic equation has one real root and two complex conjugate roots. By adapting the *conventional* design rule for random vibration control: "$\omega_{\mathrm{t}} = \omega_{\mathrm{r}}$" [18, 19], which is to tune the transition frequency ω_{t} of the mount to the resonance frequency of the fundamental vibration mode, we may now define the *general* design rule for residual vibration control considered in this paper as follows:

$$\omega_{\mathrm{t}} = \omega_{\mathrm{d}}, \tag{11}$$

where ω_{d} is the *fundamental damped natural frequency* of the complete system in free oscillation that can be given by the imaginary part of the complex conjugate roots. Mathematically, it can be seen that this is to find the solution of the third-order dynamic system in Equation (10b) satisfying the rule given by Equation (11). Here, one of the two unknowns, k and c, should be further (either explicitly or implicitly) given to yield a unique solution. As the rule literally suggests, this is also an optimization problem to maximize the loss factor $\eta(\omega)$ of the system in free oscillation, to reach $\eta_{\max}$, at ω_{d} (*Problem definition*).

Exact analytical expressions of ω_{d} are though very lengthy to handle [17]. Use of some approximates would be more intuitive and practical. Two simple approximates considered in this paper are the nominal natural frequency $\omega_{\mathrm{n}} = \sqrt{k_{\mathrm{eq}}/m_{\mathrm{a}}}$ defined earlier and the *standard natural frequency* defined now as $\omega_{\mathrm{s}} = \sqrt{k_{\mathrm{t}}/m_{\mathrm{a}}}$ in which $k_{\mathrm{t}} = kk_{\mathrm{a}}/(k + (1/2)k_{\mathrm{a}})$ is the dynamic stiffness at ω_{t} (*Approximations* I and II: fundamental vibration frequency). Using first ω_{n} for ω_{d} in Equation (11) such that $\omega_{\mathrm{t}} \approx \omega_{\mathrm{n}}$, we have

$$c_{\mathrm{opt}} \approx \frac{\left(k_{\mathrm{opt}} + k_{\mathrm{a}}\right)}{\omega_{\mathrm{a}}}. \tag{12}$$

Using then ω_{s} such that $\omega_{\mathrm{t}} \approx \omega_{\mathrm{s}}$, which is especially called the *standard* design rule in this paper, we have

$$c_{\mathrm{opt}} \approx \frac{\sqrt{\left(k_{\mathrm{opt}} + k_{\mathrm{a}}\right)\left(k_{\mathrm{opt}} + (1/2)k_{\mathrm{a}}\right)}}{\omega_{\mathrm{a}}}. \tag{13}$$

Equations (12) and (13) are approximate solutions for c_{opt} whenever k_{opt} is explicitly given. Conversely, it is also possible to obtain k_{opt} from a given c_{opt}. Accuracy of each of the two approximate solutions will be assessed later in this section.

However, a problem that still remains but is little addressed in the literature is that design tasks are rarely specified in terms of k_{opt} and c_{opt} but in terms of the bandwidth and damping requirements. We thus require some indexes to quantitatively specify these. Noting that ω_{n} and ω_{s} are readily available unlike ω_{r} and ω_{d}, we firstly propose that the system bandwidth requirement be specified by one of these (*Convention* I: bandwidth index). Consider then a truly optimal Zener mount system perfectly satisfying Equation (11). As it is now a vibration system containing m_{a}, the material property expression $\eta_{\max}$ given earlier can be rewritten as

$$\eta_{\max} = \frac{1}{2}\left[\left(\frac{\omega_{\mathrm{a}}}{\omega_{\mathrm{n}}}\right) - \left(\frac{\omega_{\mathrm{n}}}{\omega_{\mathrm{a}}}\right)\right]. \tag{14}$$

As it is also a vibration system fundamentally vibrating at ω_{t} in free oscillation because of Equation (11), $\eta_{\max}$ defined at ω_{t} can now mean the system damping property. This is called here the *effective loss factor*, denoted by $\eta_{\mathrm{e}} = \eta_{\max}$ for distinction. We thus secondly propose that the system

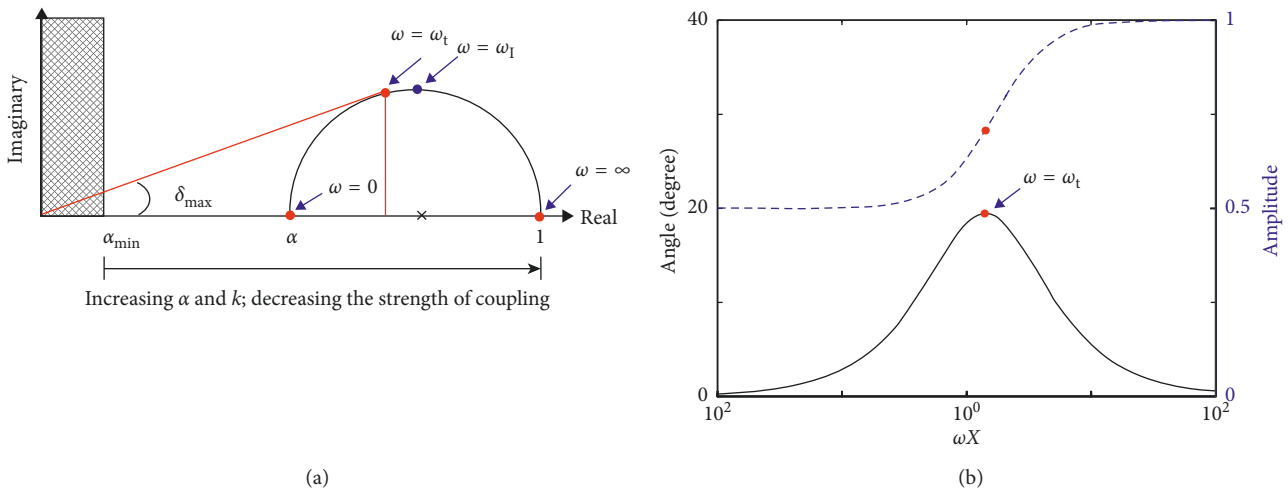

FIGURE 5: A lead compensator $C(\omega) = \alpha(1 + j\omega X)/(1 + j\alpha\omega X)$ for $\alpha = (1 + \kappa_o)^{-1}$ with $\kappa_o = 1$. (a) Polar plot and (b) amplitude (dashed line)-angle (solid) plot. The maximum loss angle δ_{max} (and η_{max}) varies according to α, where $\alpha_{min} < \alpha < 1$ in which α_{min} is determined by Equation (8).

damping requirement be specified by η_e (*Convention* II: damping index). These two conventions are valid throughout this paper.

Rewriting Equation (14) can give the generic trade-off relationship between the bandwidth and the damping requirement:

$$\frac{\omega_n}{\omega_a} = \left(\eta_e + \sqrt{1 + \eta_e^2}\right)^{-1}, \tag{15}$$

$$\frac{\omega_s}{\omega_a} = \left(\sqrt{1 + \eta_e^2 + \eta_e\sqrt{1 + \eta_e^2}}\right)^{-1}, \tag{16}$$

which also theoretically explains the trend of the simulation results in Figure 2. Referring also to Figure 5(a), it can be seen that each of these gives the maximum value k_{opt} (equivalently α_{opt}) to achieve a given level of η_e (determined by δ_{max}) or conversely the maximum value η_e under a given level of k_{opt}. Therefore, it can be finally stated that the general design rule given by Equation (11) is *practically* to yield the maximum bandwidth (the optimization goal) under a given damping requirement (the constraint) *or* conversely the maximum damping under a given bandwidth requirement of the system in free oscillation (*Problem redefinition*). It is interesting to note that the bandwidth and damping requirements of the mount are analogous to the handling and ride comfort requirements of a vehicle [26], respectively. In contrast, a suspending dynamic vibration absorber can be more easily designed without any consideration of the bandwidth (or handling) requirement [24].

Rewriting Equation (14) further gives the optimal k, whenever η_e is specified, such that

$$k_{opt} = \frac{1}{2}k_a\left(\sqrt{1 + \eta_e^{-2}} - 1\right). \tag{17}$$

It should be noted that Equations (15)–(17) are generic relations valid for all truly optimal Zener mount systems perfectly satisfying Equation (11). A specific design case for a given manipulator of mass ratio σ then imposes some limitations to the values of Equations (15)–(17) such that

$$\eta_e < \frac{\sigma}{(2\sqrt{1 + \sigma})}, \tag{18a}$$

$$k_{opt} > \frac{k_a}{\sigma}, \tag{18b}$$

$$\omega_n > \sqrt{(1 + \sigma)^{-1}}\omega_a, \tag{18c}$$

$$\omega_s > \sqrt{\left(1 + \frac{\sigma}{2}\right)^{-1}}\omega_a, \tag{18d}$$

all because of the condition given by Equation (8).

Figure 6 displays a curve (thick line) representing Equation (16) and an area (shaded area) confined by Equation (18) for a manipulator of $\sigma = 6.86$. Equation (15) may alternatively be used to draw the curve. The curve is called here the *optimal design curve*, while the area is the *design region*. The curve is invariant while the area enlarges as σ increases. The bandwidth and damping requirements can then be specified at a point along the optimal design curve within the design region. It subsequently gives the exact solution for k_{opt} as explicitly given by Equation (17). The corresponding D gain c_{opt} can then be approximately determined by Equations (12) or (13). It is desirable that the manipulator is of a sufficiently large mass ratio σ so that its design region includes a critical value of η_e (e.g., $\eta_e = 1$) giving the critical damping. This is often satisfied in many practical flexible manipulators (e.g., $\sigma > 5$).

3.3. Simulations. Simulations were performed to compare Equations (12) and (13) by using the two-body LES in Figure 1(b). The data used and the three design cases ($\eta_e = 0.3$, 0.5, and $1/\sqrt{2}$) considered are given in Tables 1 and 2, respectively. The three effective loss factors η_e

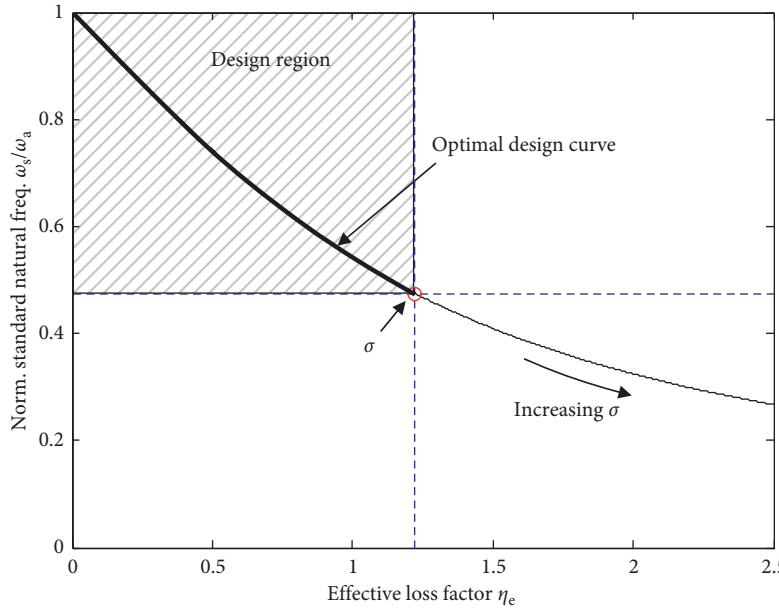

Figure 6: Generic optimal design curve (thick line) in the specific design region (shaded area) for a given manipulator of the mass ratio $\sigma = 6.86$. The system bandwidth and damping requirements are represented by ω_s/ω_a and η_e, respectively.

Table 1: Identified lumped elements of the mechanical manipulator.

Base mass, m (kg·m^2)	Mass ratio, $\sigma = m_a/m$	Appendage spring, k_a (N·m/rad)	Appendage natural frequency, $\omega_a/(2\pi)$ (Hz)	Appendage damping ratio, ζ_a
3.83×10^{-4}	6.86	9.744	9.7	0.01

Table 2: Three test cases with their optimal P and D gains.

η_e	ω_b/ω_a	$\omega_s/2\pi$ (Hz)	$\omega_d/2\pi$ (Hz)	k_{opt} from Equation (17)	c_{opt} from Equation (12)	c_{opt} from Equation (13)	c_{opt} satisfying Equation (11)
0.3	2.92	8.19	8.26	12.082	0.358	0.316	0.313
0.5	2.06	7.21	7.37	6.022	0.259	0.215	0.211
$1/\sqrt{2}$	1.58	6.31	6.55	3.568	0.218	0.174	0.168

Note. Unlike the other terms, "$\omega_d/(2\pi)$" and "c_{opt} satisfying Equation (11)" were numerically obtained. Here, "$\omega_d/(2\pi)$" was calculated from "k_{opt} from Equation (17)" and "c_{opt} satisfying Equation (11)." Units: k_{opt} (N·m/rad); c_{opt} (N·m·s/rad).

specified are all within the valid design region since $\omega_b/\omega_a > 1$ as indicated in Table 2. The optimal design curve, equivalently Equations (15)–(17), yielded ω_s and k_{opt} for each case. The gain c_{opt} was then obtained by Equations (12) and (13).

Figure 7(a) shows the resulting tip responses in frequency, calculated from Equations (5) and (6). It can be seen that ω_s (denoted by "o") estimates ω_d (denoted by "∇") better than ω_n (denoted by "+") does, where each ω_d indicated was numerically obtained from the roots of Equation (10) ("roots" in Matlab®). The deviation gets larger as η_e increases. It is clear from the simulations that Equation (13) is more accurate than Equation (12). Consequently, the responses obtained from Equation (13) should more closely resemble the true optimal performances intended (Appendix B). Figure 7(b) then shows the corresponding tip responses in time excited by a step motion input, illustrating now the relationship between η_e and the settling time. It can be seen that the responses for $\eta_e = 1/\sqrt{2}$ (lower pair), which is $\eta_e < 1$, are already quite highly damped.

Overall, a Zener mount design methodology based on the performance indexes of ω_s and η_e has been established to analytically determine the optimal P and D gains: Equations (17) and (13) confined by Equation (18), respectively. Here, the design methodology also represented by Figure 6 together with Approximation II and Conventions I and II is an important contribution of this paper. A merit of this is that the optimal gains are determined without actually solving the cubic equation in Equation (10b) subject to Equation (11). The P gain obtained is the exact solution (satisfying $\omega_t = \omega_d$), while the D gain is a suboptimal solution (satisfying $\omega_t = \omega_s$). The D gain can be very close to its exact solution if $\omega_d \approx \omega_s$, which is often satisfied when the damping requirement is not highly demanded; for example, $\eta_e < 1$ (Table 2 and Appendix B). It should be finally emphasized that the design methodology presented in this paper is also applicable to various

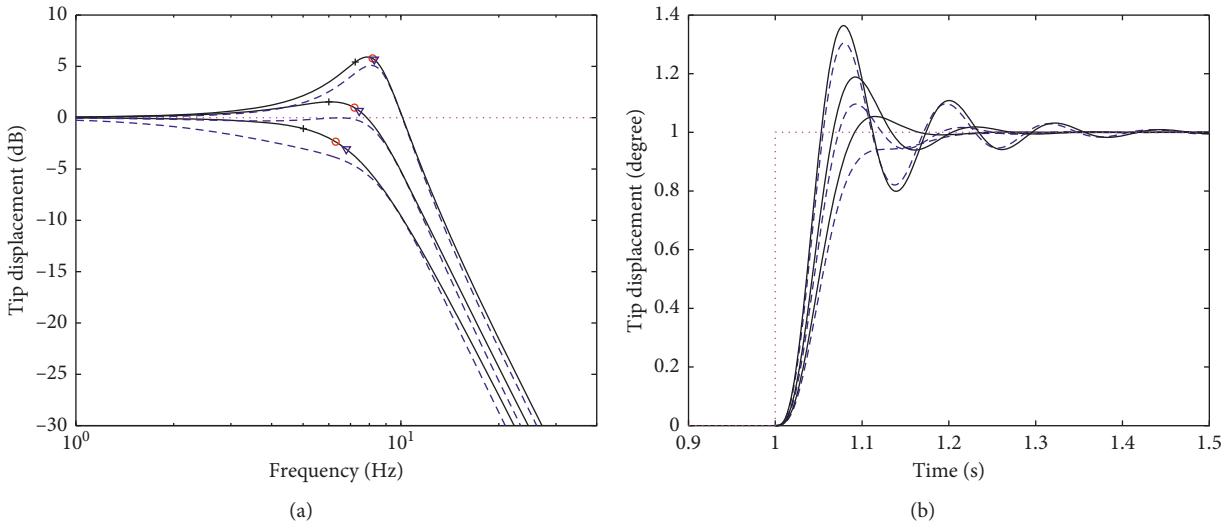

FIGURE 7: Predicted tip displacements: (a) the frequency responses from Equation (12) (dashed lines) and Equation (13) (solid) for three test cases: $\eta_e = 0.3$ (upper pair), 0.5 (middle), and $1/\sqrt{2}$ (lower). The symbols, "+," "o," and "∇" are indicated at the nominal natural frequency ω_n, the standard natural frequency ω_s, and the damped natural frequency ω_d in successive order. The dotted line indicates the command input signal. (b) The corresponding time responses to a step input.

forms of Zener mount design problems in the field of vibration isolation. Its application can further extend to various forms of vehicle suspension design problems because the model in Figure 3(a) is dynamically the same as the quarter-car model having a negligible unsprung mass [27]. Both models are indeed governed by the same characteristic equation given by Equation (10).

4. Experiments

4.1. Experimental Setup and Modeling. The experimental setup driving a single-link flexible beam in the horizontal plane is shown in Figure 8. An AC servo motor (Yaskawa® SGMJV-02ADA2C, 200 Watts) was directly connected to the beam (1 mm × 25 mm × 270 mm) of spring steel, without the use of a reduction gear. A built-in 20-bit incremental encoder equipped within the motor was used to measure the rotation angle. An accelerometer was additionally attached to the end tip of the beam to monitor the vibration. A servo drive (Yaskawa® SGDV 1R6A01A) was used in "torque control mode" so as to act as a current amplifier, producing a mechanical motor torque output in proportional to the electrical drive voltage input. Consequently, the back electromotive force effect of the motor could have been excluded in the servo drive mechanism. The diagram in Figure 8 is thus exactly analogous to that in Figure 1(a) but merely described in terms of voltages and the dimensionless gains, K_p and K_v. The control circuit was implemented within a real-time prototyping machine (Matlab/Simulink xPC target module) running at a sampling frequency of 16 kHz.

To model the mechanical manipulator, a random signal V_{dis} was supplied with the controller being deactivated (i.e., $K_p = K_v = 0$). The time derivative (i.e., velocity) of the measured encoder angle response to this excitation, which is termed the driving point mobility, is compared in Figure 9(a) with its identification using Equation (4) with setting $k = c = 0$. Although the mobility is displayed by convention, the impedance (i.e., the inverse of the mobility data) is of importance for the curve-fitting in the LEM [12–14]. Thus, it can be seen that the first antipeak of the mobility has been closely fitted. The lumped elements identified are already tabulated in Table 1. The measured transmissibility is then compared in Figure 9(b) with the simulation using Equation (3). The measured response was obtained by dividing the tip angle motion by the hub angle motion, where the tip angle motion was obtained by dividing the tip translational displacement (double integral of the acceleration measured by the accelerometer) by the arm length. Here, the double integration means dividing the acceleration response by $(j\omega)^2$ in the frequency domain. The angle motions can be regarded as the generalized displacements indicated in Figure 1(b). Note that the use of the accelerometer was not for the modeling but merely for monitoring the tip motion. It can be seen in Figures 9(a) and 9(b) that the simulated responses from the semidefinite LES agree well with the measured responses at very low and low frequencies. The peaks higher than the first one in Figure 9(b) are the higher modes of the beam [13], which were deliberately unmodeled in this paper as they are unimportant under Condition II.

4.2. Experimental Performance. The three control cases listed in Table 2 were then experimentally tested. The values of "c_{opt} from Equation (12)" in the table were solely used for the D gains throughout the control experiments. (This was because Equation (13) has been only recently developed while finalizing this paper.) The experimental results obtained are still useful to validate the complete LES model (now containing k_{opt} and c_{opt}) and further to investigate any unforeseen dynamics and instability issues in real

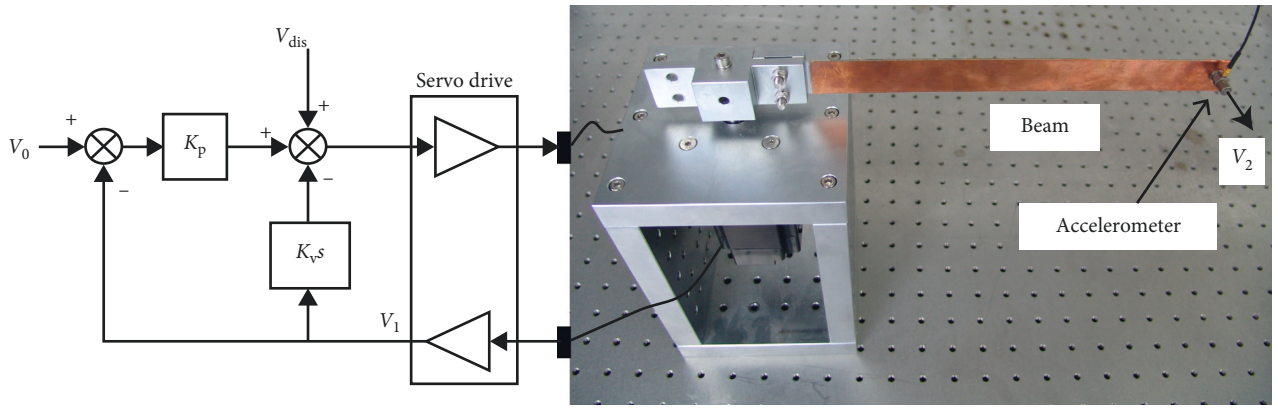

Figure 8: Experimental setup for a PD-controlled servo system driving a single-link flexible beam.

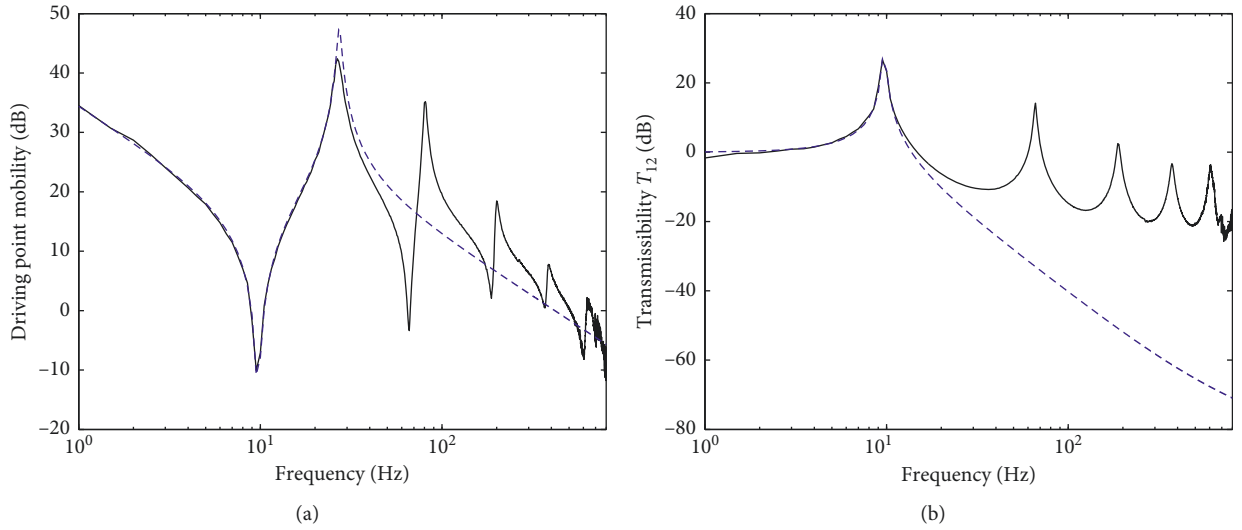

Figure 9: Measured (solid lines) responses of the flexible manipulator and their identifications (dashed) using the semidefinite two-body LES ($k = c = 0$): (a) the driving point mobility and (b) the vibration transmissibility T_{12} from the hub to the tip.

applications. The control behavior was first examined in the frequency domain by supplying a random signal to V_{dis}, while setting $V_0 = 0$ in Figure 8. To validate the LES model, the generalized hub and tip displacements (solid lines) for the case of $\eta_e = 0.5$ are compared in Figures 10(a) and 10(b), respectively, with their predictions (dashed) calculated from Equations (5) and (6). They agree well at low frequencies particularly for the fundamental vibration mode at around 7 Hz. Some slight deviations at very low frequencies are thought to be due to friction in the motor that was neglected in the model but becomes influential for slow motion [28].

The measured hub and tip responses for all three cases are then compared in Figures 11(a) and 11(b) to clearly demonstrate the damping effect η_e. An additional case was also tested using an arbitrarily large $k = 50$ (N·m/rad) and a small $c = 0.03$ (N·m·s/rad), and the results (thick dotted) are also overlaid to illustrate how large vibrations could be induced when the gains were inappropriately chosen [7, 13].

The performance of the control system was finally examined in the time domain but now with a step input of 20° to the reference input V_0 while setting $V_{dis} = 0$. The hub displacements and the tip accelerations for the three test cases are compared in Figures 12(a) and 12(b), respectively. The additional case considered in Figure 11 could not be tested because of the limitation of the output voltage of the controller used. The trend in the step responses is similar to that in the frequency response functions in Figure 11. A small offset error is also evident when the P gain was small (i.e., a soft spring), for example, $\eta_e = 1/\sqrt{2}$.

Throughout the control experiments described above, no instability was encountered. This was not because the experimental control system was genuinely passive like the theoretical LES model presented but because only moderate gains were implemented for the optimal PD controllers designed under Condition II. If very large gains had to be used for some other requirements, the system could indeed go unstable because of the time delay (approx. 0.5 ms: measured) inherent within the servo drive used. This time

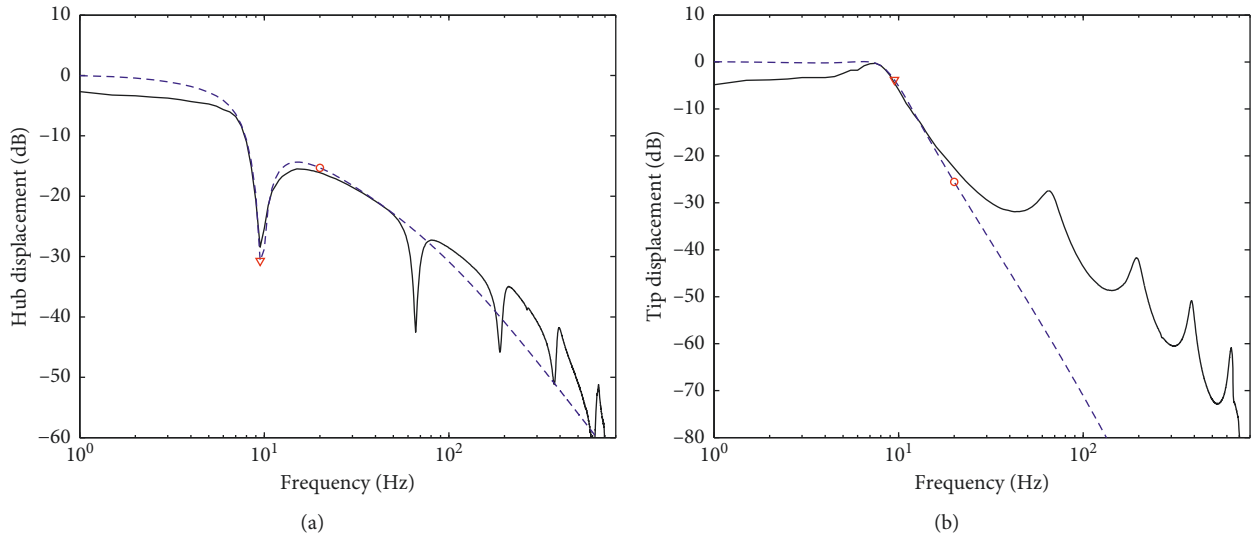

FIGURE 10: Measured (solid lines) responses of the manipulator system for $\eta_e = 0.5$ and their predictions (dashed) using the positive-definite two-body LES ($k \neq c \neq 0$): (a) the hub displacement T_{01} and (b) the tip displacement T_{02}. The symbols, "∇" and "o," are indicated at the uncoupled appendage and base natural frequencies, ω_a and ω_b, respectively.

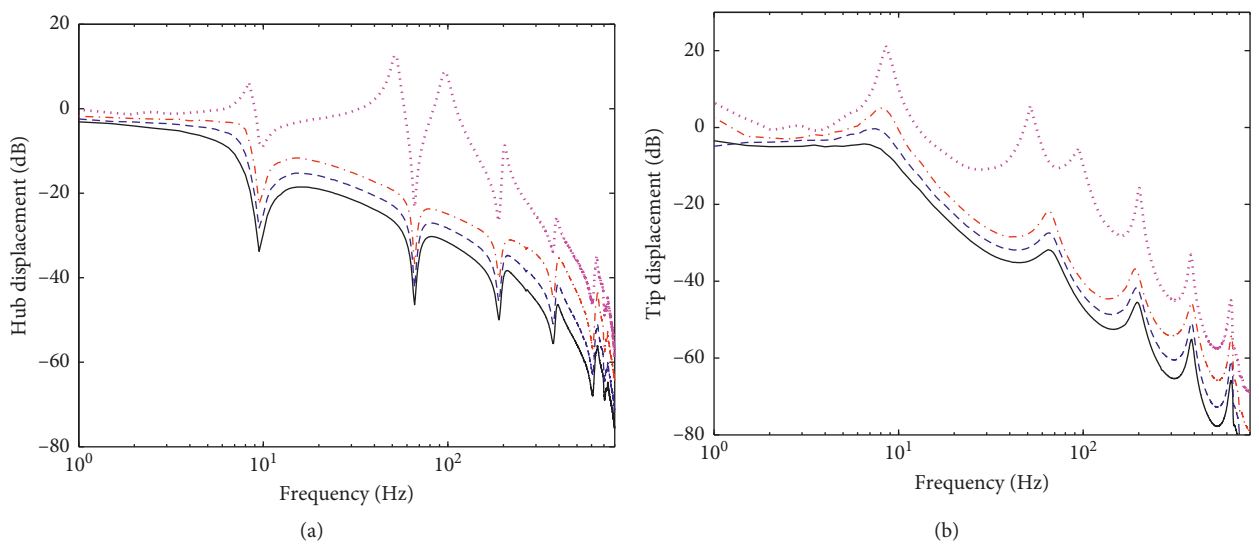

FIGURE 11: Measured responses for the three control cases, $\eta_e = 0.3$ (dashed dotted line), 0.5 (dashed), $1/\sqrt{2}$ (solid), and an additional case with arbitrary gains (thick dotted): (a) the hub displacement and (b) the tip displacement.

delay is also that can cause a rapid rigid manipulator system unstable [11].

Overall, the experimental results obtained have been presented to verify the LES model developed. It has also demonstrated that some friction-induced offset error can be persistent if a soft (a small k) manipulator system is operating slowly. Such error could be effectively reduced by using a large k *or* completely eliminated by introducing an integral action within the controller, becoming then a PID controller. Although this paper is specifically concerned with the PD controller of a linear flexible manipulator system, it should be emphasized that the optimal P and D gains presented can still be used, at least, as initial values of an intelligent PID controller for a flexible manipulator of unknown friction dynamics [29]. More fundamentally, the mathematical logic and physical insights presented in this paper provide a basic foundation upon which an analytical PID-tuning method can be established in the future for general nonlinear manipulator systems.

5. Conclusions

A seemingly complex but fundamental problem in the field of motion control has been tackled, which is to analytically tune the PD controller of a linear flexible manipulator system. More specifically, the problem is to give simple closed-form solutions of the optimal P and D gains to yield the maximum bandwidth under a given damping requirement *or* conversely the maximum damping under a given bandwidth requirement of the system in free

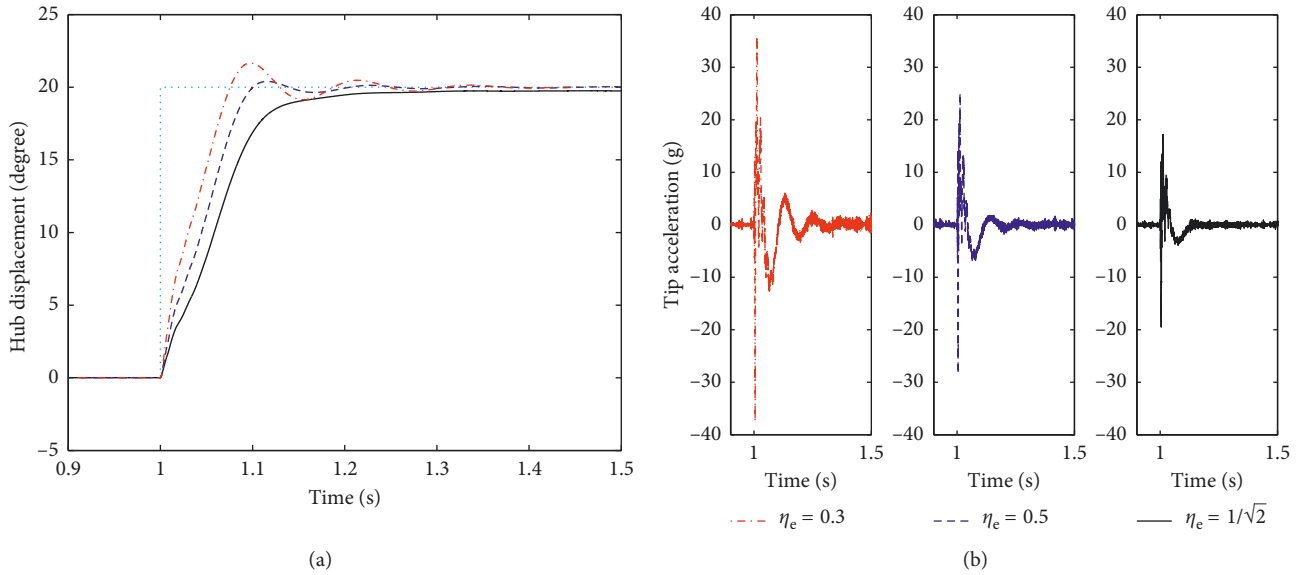

FIGURE 12: Measured responses to a step input (dotted) of 20° for the three test cases: $\eta_e = 0.3$ (dashed dotted line), 0.5 (dashed), and $1/\sqrt{2}$ (solid): (a) the hub displacement and (b) the tip acceleration.

oscillation. It has turned out that the original servo control problem is analogous to a conventional Zener mount design problem. A design methodology has been finally established to analytically determine the optimal elements of the mount, corresponding to the optimal control gains. The P gain obtained is the exact optimal solution while the D gain is a suboptimal solution that can also be very close to its exact solution if the damping requirement is not highly demanded. The D gain can further be nearly exactly tuned, regardless of the damping requirement, if a numerical frequency tuning method is allowed. Mathematically, it should be emphasized that the methodology established in this paper offers an optimal design solution to a third-order dynamic system. Practically, it can thus be applied to various dynamic systems including Zener mounts and vehicle suspensions in the field of vibration isolation.

Appendix

A. Some Important Frequencies

With reference to the system in Figure 1(b), the appendage and base angular natural frequencies are, respectively,

$$\omega_a = \sqrt{\frac{k_a}{m_a}}, \qquad \omega_b = \sqrt{\frac{k}{m}}. \tag{A.1}$$

With reference to the system in Figure 3(a), the nominal and standard angular natural frequencies of the Zener mount system are, respectively,

$$\omega_n = \sqrt{\frac{k_{eq}}{m_a}}, \qquad \omega_s = \sqrt{\frac{k_t}{m_a}}, \tag{A.2}$$

where $k_{eq} = kk_a/(k + k_a)$ is the static stiffness while $k_t = kk_a/(k + (1/2)k_a)$ is the dynamic stiffness at the transition frequency of the Zener mount given by

$$\omega_t = (\sqrt{\alpha}\, X)^{-1}, \tag{A.3}$$

where $\alpha = (1 + \kappa)^{-1}$, $\kappa = k_a/k$, and $X = c/k$. With reference to the frequency responses in Figures 2, 7(a), 10, and 11, the first peak frequency of each response is defined as the resonance frequency ω_r of the fundamental vibration mode of the corresponding servo system in operation under a certain *steady-state* excitation. With reference to the time responses in Figures 7(b) and 12, the fundamental residual vibration frequency is defined as the fundamental damped natural frequency ω_d of the servo system in *free* oscillation.

B. Alternative Approaches Using Analytical Convex Minimization and Numerical Frequency Tuning

The two design cases studied in this Appendix are depicted in Figures 13(a) and 13(b), where the system in Figure 13(a) is subjected to a motion input x_0 on both k and c, while that in Figure 13(b) is on k only. The system in Figure 13(b) is the same as that considered in the main text. The dynamic equations of the first case can be written in the Laplace domain $s = j\omega$ as

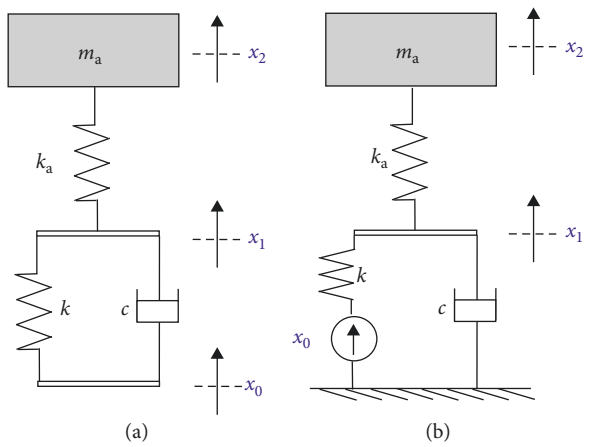

FIGURE 13: Two design cases: (a) $k\|c$ excitation and (b) k-only excitation.

$$\left(m_a s^2 + k_a\right)x_2 - k_a x_1 = 0, \tag{B.1a}$$

$$\left(k_a + k + cs\right)x_1 = k_a x_2 + (k + cs)x_0. \tag{B.1b}$$

The vibration transmissibility function from x_0 to x_2 is then given by

$$T_{02} = \frac{1 + j2\zeta\kappa r}{1 - (1+\kappa)r^2 + j2\zeta\kappa r\left(1 - r^2\right)}, \tag{B.2}$$

where $\kappa = k_a/k$, $r = \omega/\omega_a$, and $\zeta = c/(2m_a\omega_a)$. Given the value of κ, the design problem here is to find ζ_{opt} and r_{opt} that minimize the resonant vibration amplitude of T_{02} such that

$$J_{min} = \min(\max(J)) \quad \text{for all } \zeta \text{ and } r, \tag{B.3}$$

where $J = |T_{02}| = \sqrt{N/D}$ in which $N = 1 + (2\zeta\kappa r)^2$ and $D = (1 - (1+\kappa)r^2)^2 + (2\zeta\kappa r(1-r^2))^2$. Under the assumption that the function J has the global minimum, we can apply the convex minimization scheme [30] $\partial J^2/\partial\zeta = 0$ to get $D = N(1-r^2)^2$ and consequently $r_{opt} = 1/\sqrt{1+\kappa/2}$. It finally turns out that the resonance frequency solution is $\omega_{r,opt} = \omega_s$, which is *surprisingly* the same as the standard natural frequency defined in the main text. We can then apply $\partial J^2/\partial r = 0$ to get $\zeta_{opt} = \sqrt{(1+\kappa)(1+\kappa/2)}/(2\kappa)$ and consequently c_{opt} that is the same as Equation (13). The global minimum for each κ is then given by

$$J_{min} = 1 + \frac{2}{\kappa}, \tag{B.4}$$

where it can be seen that it is always $J_{min} > 1$ for all positive κ.

It is further interesting that the vibration transmission problem here through a series-type Zener mount is exactly analogous to the force transmission problem through a parallel-type Zener mount widely studied in a textbook [30] and also in Reference [17]. In these standard cases to which the convex minimization scheme is applicable, the conventional design rule ($\omega_t = \omega_r$) turns into the *standard* design rule defined in Section 3.2 as

$$\omega_t = \omega_s. \tag{B.5}$$

Under the optimal design framework defined mathematically by Equation (B.3) or intuitively by Equation (B.5), not only the P gain in Equation (17) but the D gain in Equation (13) is also the exact solution for the particular system shown in Figure 13(a). Strictly speaking, this framework is concerned with the steady-state vibration under a certain excitation condition while the *general* design rule given by Equation (11) is with any residual transient vibration. However, these two rules often yield similar results in many practical applications. This might be a reason why they were not clearly distinguished from one another in the literature [18, 19].

Similarly, the transmissibility function of the second case in Figure 13(b) can be written as

$$T_{02} = \frac{1}{1 - (1+\kappa)r^2 + j2\zeta\kappa r\left(1 - r^2\right)}. \tag{B.6}$$

Applying again $\partial J/\partial\zeta = 0$ now gives a trivial solution, which means that the convex minimization scheme is no longer applicable. In this nonstandard case, some approximate solutions would be more appropriate as illustrated below with simulations.

The standard and general design rules, respectively, given by Equations (B.5) and (11), were applied to the two systems in Figure 13 for the three design cases listed in Table 2. The P gain was analytically determined by Equation (17) for both rules. The D gain of the standard rule was then analytically determined by Equation (13), which is also the solution of the convex optimization method earlier. However, that of the general rule was numerically (i.e., iteratively) tuned until it precisely met the frequency tuning condition in Equation (11), which is a numerical frequency tuning method. The optimal D gains finally tuned (i.e., "c_{opt} satisfying Equation (11)") are also added to Table 2 for comparison. It can be seen that if either of the two rules is applied and if the damping requirement is not highly demanded, we have

$$\omega_s \approx \omega_d \quad \text{if } \omega_t = \omega_d \text{ or } \omega_t = \omega_s \text{ and if } \eta_e < 1, \tag{B.7}$$

and consequently the values of c_{opt} from Equations (13) and (11) are also very similar to each other, justifying Approximation II of the main text.

Using the values of k_{opt} and c_{opt} obtained as tabulated in Table 2, the generalized tip displacements of the two systems in Figures 13(a) and 13(b) could finally be calculated as shown in Figure 14. Those fulfilling the general (solid lines) and standard (dashed) rules are displayed together for comparison. Some symbols are additionally indicated to confirm that the rules have been correctly applied. It can be seen that ω_d (indicated by "∇" in the graphs of the k-only excitation case, for convenience) and ω_s (indicated by "+" in the graphs of the $k\|c$ excitation case) coincide with their corresponding values of ω_t (indicated by "o" in the graphs of both cases), respectively. It can also be seen that little is discernable between each pair (solid and dashed lines) of the responses, particularly when η_e is small. This supports that the simple standard rule ($\omega_t = \omega_s$) can be used instead of the

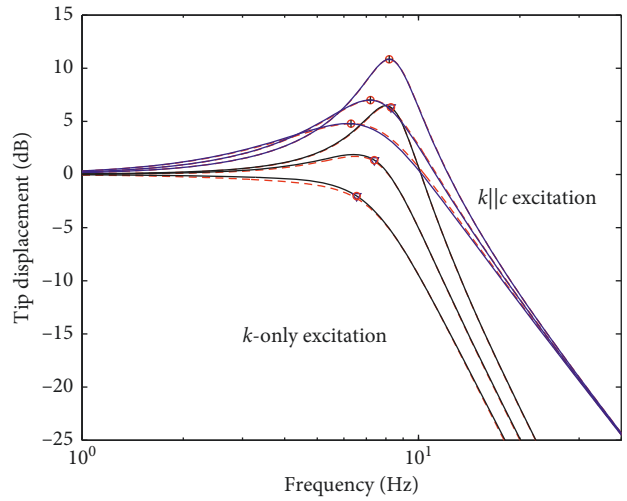

FIGURE 14: Optimal responses using the general design rule "$\omega_t = \omega_d$" (solid lines) and the standard design rule "$\omega_t = \omega_s$" (dashed) for the two systems in Figure 13 in three different design cases given by Table 2. The symbols, "o," "+," and "∇" are indicated at ω_t, ω_s, and ω_d in successive order.

general rule ($\omega_t = \omega_d$), if the damping requirement is not highly demanded. Thus, the analytical design methodology presented in this paper can be applied to many practical residual as well as random vibration control problems, where $\eta_e < 1$ so that $\omega_d \approx \omega_r \approx \omega_s$.

Data Availability

The data used to support the findings of this study are available from the corresponding author upon request.

Conflicts of Interest

The authors declare that there are no conflicts of interest regarding the publication of this paper.

Acknowledgments

This research was commenced in 2011 and was partly supported by the Leading Human Resource Training Program of Regional Neo Industry through the National Research Foundation of Korea (NRF) funded by the Ministry of Science, ICT, and Future Planning (No. 2016H1D5A1910490).

References

[1] A. De Luca and W. Book, "Robots with flexible elements," in *Handbook of Robotics*, B. Siciliano and O. Khatib, Eds., pp. 287–319, Springer, Berlin, Germany, 2008.

[2] K. Ogata, *Modern Control Engineering*, Prentice Hall, Inc., Upper Saddle River, NJ, USA, 1970.

[3] V. Parra-Vega, S. Arimoto, Y.-H. Liu, G. Hirzinger, and P. Akella, "Dynamic sliding PID control for tracking of robot manipulators: theory and experiments," *IEEE Transactions on Robotics and Automation*, vol. 19, no. 6, pp. 967–976, 2003.

[4] J. Y. Hung, "Posicast control past and present," *IEEE Multidisciplinary Engineering Education Magazine*, vol. 2, pp. 7–11, 2007.

[5] Z. Mohamed, J. M. Martins, M. O. Tokhi, J. Sá da Costa, and M. A. Botto, "Vibration control of a very flexible manipulator system," *Control Engineering Practice*, vol. 13, no. 3, pp. 267–277, 2005.

[6] A. J. Fleming and K. K. Leang, *Design, Modeling and Control of Nanopositioning Systems*, Springer, New York, NY, USA, 2014.

[7] S. M. Kim, H. Kim, K. Boo, and M. J. Brennan, "Demonstration of non-collocated vibration control of a flexible manipulator using electrical dynamic absorbers," *Smart Materials and Structures*, vol. 22, no. 12, article 127001, 2013.

[8] P. Tomei, "A simple PD controller for robots with elastic joints," *IEEE Transactions on Automatic Control*, vol. 36, no. 10, pp. 1208–1213, 1991.

[9] C. Yang, Q. Huang, H. Jiang, O. O. Peter, and J. Han, "PD control with gravity compensation for hydraulic 6-DOF parallel manipulator," *Mechanism and Machine Theory*, vol. 45, no. 4, pp. 666–677, 2010.

[10] T. H. Lee, K. K. Tan, and S. Huang, "Adaptive friction compensation with a dynamical friction model," *IEEE/ASME Transactions on Mechatronics*, vol. 16, no. 1, pp. 133–140, 2011.

[11] K. J. Åström and T. Hägglund, "The future of PID control," *Control Engineering Practice*, vol. 9, no. 11, pp. 1163–1175, 2001.

[12] S. M. Kim, "Lumped element modeling of operational structures by inverting the mobility models," *Mechanical Systems and Signal Processing*, vol. 49, no. 1-2, pp. 106–117, 2014.

[13] S. M. Kim, "Lumped element modeling of a flexible manipulator system," *IEEE/ASME Transactions on Mechatronics*, vol. 20, no. 2, pp. 967–974, 2015.

[14] S. M. Kim, "On the dual side of operational dynamics: a formulation, applications, and implications of the impedance model," *Journal of Sound and Vibration*, vol. 364, pp. 207–221, 2016.

[15] B. Wie and D. S. Bernstein, "Benchmark problems for robust control design," *Journal of Guidance, Control, and Dynamics*, vol. 15, no. 5, pp. 1057–1059, 1992.

[16] F. Mainardi and G. Spada, "Creep, relaxation and viscosity properties for basic fractional models in rheology," *European Physics Journal*, vol. 193, no. 1, pp. 133–160, 2011.

[17] M. J. Brennan, A. Carrella, T. P. Waters, and V. Lopes Jr., "On the dynamic behaviour of a mass supported by a parallel combination of a spring and an elastically connected damper," *Journal of Sound and Vibration*, vol. 309, no. 3–5, pp. 823–837, 2008.

[18] M. Sugino and S. Takehara, "Method of determining and damping vibrations," United States Patent 4,779,853, 1998.

[19] J. H. Lee and K. J. Kim, "A method of transmissibility design for dual-chamber pneumatic vibration isolator," *Journal of Sound and Vibration*, vol. 323, no. 1-2, pp. 67–92, 2009.

[20] E. L. Hixson, "Chapter 10—mechanical impedance," in *Shock and Vibration Handbook*, C. M. Harris, Ed., McGraw Hill, New York, NY, USA, 3rd edition, 1987.

[21] S. M. Kim and M. J. Brennan, "A compact matrix formulation using the impedance and mobility approach for the analysis of structural-acoustic systems," *Journal of Sound and Vibration*, vol. 223, no. 1, pp. 97–113, 1999.

[22] S. M. Kim and M. J. Brennan, "Modeling a structural–acoustic coupled system with an equivalent lumped parameter mechanical system," *Journal of Vibration and Acoustics*, vol. 121, no. 4, pp. 453–459, 1999.

[23] C. E. Crede and J. E. Ruzicka, "Chapter 30—theory of vibration isolation," in *Shock and Vibration Handbook*,

C. M. Harris, Ed., McGraw Hill, New York, NY, USA, 3rd edition, 1987.

[24] S. M. Kim, "Turning a loudspeaker into an active Helmholtz resonator: underlying law, principle and design methodology," *Journal of Sound and Vibration*, vol. 432, pp. 373–386, 2018.

[25] M. Carfagni, E. Lenzi, and M. Pierini, "The loss factor as a measure of mechanical damping," in *Proceedings of the 16th International Modal Analysis Conference, Paper No. 3243*, pp. 580–584, Santa Barbara, CA, USA, February 1998.

[26] P. S. Els, N. J. Theron, P. E. Uys, and M. J. Thoresson, "The ride vs. handling compromise for off-road vehicles," *Journal of Terramechanics*, vol. 44, no. 4, pp. 303–317, 2007.

[27] T. D. Gillespie, *Fundamentals of Vehicle Dynamics*, Society of Automotive Engineers, Inc., Warrendale, PA, USA, 1992.

[28] P. E. Dupont and E. P. Dunlap, "Friction modeling and PD compensation at very low velocities," *Journal of Dynamic Systems, Measurement, and Control*, vol. 117, no. 1, pp. 8–14, 1995.

[29] J.-W. Jung, V. Q. Leu, T. D. Do, E.-K. Kim, and H. H. Choi, "Adaptive PID speed control design for permanent magnet synchronous motor drives," *IEEE Transactions on Power Electronics*, vol. 30, no. 2, pp. 900–908, 2015.

[30] D. J. Inman, *Engineering Vibration*, Pearson, New York, NY, USA, 4th edition, 2014.